

X rays from laser-fired microspheres

N. G. Basov, G. A. Vergunova, E. G. Gamaliĭ, V. A. Gasilov, N. N. Demchenko, A. I. Isakov, A. A. Kologrivov, Yu. A. Merkul'ev, V. B. Rozanov, A. A. Samarskiĭ, G. V. Sklizkov, V. F. Tishkin, A. P. Favorskiĭ, and A. S. Shikanov

P. N. Lebedev Physics Institute, USSR Academy of Sciences
(Submitted 15 June 1982)

Zh. Eksp. Teor. Fiz. **84**, 564–575 (February 1983)

The x rays from gas-filled target shells irradiated by nanosecond laser pulses in the “pusher shell” regime are investigated. Various methods are used to study the spectral distribution of the continuous x radiation in experiments on the “Kal'mar” facility, and the volume compression is measured. A numerical simulation of the compression process has made it possible to obtain the spectrum of the target's own radiation and the image of the target in its own x rays. The hardest part of the spectrum is strongly influenced by difference between the distribution in the degree of ionization and the thermodynamic equilibrium distribution, and by the presence of hard electrons in the corona. The experimental results agree with the numerical calculations, thereby confirming the earlier conclusion that the hydrodynamic model with classical transport coefficient is valid.

PACS numbers: 52.50.Jm, 52.25.Ps

INTRODUCTION

The purpose of the theoretical and experimental investigations of heating and compression of spherical targets by laser radiation is to choose the optimal compression regime, i.e., to choose a laser + target system providing a positive energy yield. Recent investigations have shown convincingly that this regime is the “pusher shell” regime (sometimes called the ablation regime) at a relatively low heating-radiation flux density $q \lesssim 10^{14}$ W/cm² (Ref. 1). We recall that even the first experiments² that followed the theoretical studies³ confirmed the possibility of attaining high degrees of matter compression in this regime.

The present paper is devoted to a theoretical and experimental study of x rays from laser-fired spherical targets, in connection with the experiments of the nine-channel “Kal'mar” laser facility.⁴ The study of the x rays is part of an all-inclusive research program; this paper is therefore a continuation of a number of papers^{1,5} devoted to the study of the absorption and refraction of the laser radiation in the target “corona,” and to the hydrodynamic processes in the corona and during the compression stage. Naturally, the present paper is connected with the preceding ones also by the unity of the physico-mathematical model used to describe the processes in the plasma, but we supplement here the earlier numerical codes by new ones in which account is taken of the generation and transport of the x rays, the evolution of the x-ray spectra, and the passage of the x rays through the recording system (the RIM program).

X-ray diagnostics is one of the effective experimental methods of determining laser-plasma parameters.⁶ In the present paper we investigate in a wide spectral range ($\hbar\omega \lesssim 20$ keV) the spectral distribution of the continuous x radiation. This distribution can yield the average plasma temperature and the effective “temperature” of the non-Maxwellian tail of the fast electrons. Investigation of the plasma soft-x-ray luminosity is carried out with the aid of multichannel pinhole cameras at high spatial resolution.

Comparison of the experimentally obtained images of

the targets in their own x rays with those obtained by numerical simulation yields an estimate of the volume compression of the gas.

§1. PHYSICAL MODEL

It is known⁷ that when glass shell targets are compressed at an absorbed-energy 20–40 J the plasma electron temperature does not exceed 1 keV. Under these conditions the x rays from the target are due mainly to free-free and free-bound transitions (bremsstrahlung and recombination radiation) with a relatively small contribution of bound-bound transition (emission in the lines).

In addition, resonant anomalous absorption causes the so-called fast electrons to be generated in the laser plasma, and this leads to a deviation of the electron distribution from Maxwellian. The physical model for the description of the heating and compression processes includes equations for the absorption of the incident radiation and the equations of single-fluid two-temperature hydrodynamics with classical electron thermal conductivity and ion viscosity in the one- or two-dimensional approximation. This model was realized in the Luch,⁸ Rapid,⁹ and ASAF¹⁰ programs, in which the x-rays are taken into account in the total energy balance only in the form of volume losses. In this model the fraction of the intrinsic plasma radiation does not exceed 5%.

To obtain the space-time radiation field it is necessary to add to the aforementioned equations the spectral radiation transport equations with the sources indicated above, as well as the equations that describe the space-time picture of the ionization.

The characteristic ionization times in the corona of a laser target turn out to be of the same order as the heating time and the time of hydrodynamic compression and expansion, so that the ionization process is nonequilibrium and nonstationary.¹⁰ The evolution of the ionization makeup of the plasma will be described here by the following system of equations^{11,12}:

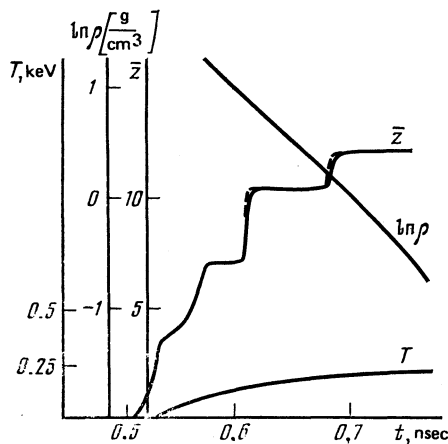


FIG. 1. Time variation of the average charge \bar{z} of silicon as a function of the density ρ and of the temperature T during the stage of formation of the corona of a glass target (dashed curve—behavior of \bar{z}_{st}).

$$\frac{dn_z}{dt} = n_{z-1}v_{ion}^{z-1} - n_z(v_r^z + v_w^z + v_{ion}^z) + n_{z+1}(v_r^{z+1} + v_w^{z+1}), \quad (1)$$

where n_z is the density of the ions with charge z ; v_{ion}^z is the rate of ionization by electron impact of an ion with charge z ; v_r^z and v_w^z are the rates of recombination in triple collisions and of the photorecombination. Equation (1) leads in the stationary case, at high density, to an equilibrium Saha distribution ($v_r^z \gg v_w^z$, the Saha distribution takes place in the cores of the targets), and in the other limiting case to a coronal equilibrium that is realized in the rarefied hot corona of the targets ($T_e \gtrsim 0.1$ keV, $n_e \lesssim 10^{22}$ cm $^{-3}$). The ionization is nonstationary during the stage of corona formation when its temperature is increased to 0.3 keV.

Figure 1 shows for silicon the average charge \bar{z} calculated as a function of time for typical density $\rho(r, t)$ and temperature $T(r, t)$ dependences in the formation of the corona of a glass target irradiated by a flux $q \approx 10^{14}$ W/cm 2 . In this case the nonstationary character of the ionization is important only for the silicon K shell. Its influence on the emission of the intrinsic radiation is insignificant and can manifest itself after a time $\sim 10^{-11}$ sec (within this time \bar{z} becomes equal to \bar{z}_{st} , which is determined from (1) under the condition $dn_z/dt = 0$). In targets containing atoms with large z , the nonstationarity and disequilibrium of the ionization can lead to an appreciable difference between the average charge \bar{z} and the equilibrium value at the given instant of time.

The emissivity per unit volume of the plasma at the point r in the direction Ω at a frequency ω , with allowance for the disequilibrium and nonstationarity of the ionization, is given by

$$e_\omega = I_{\omega p} \left\{ \sum_{z, \gamma} k_{z\gamma} \frac{1 + \bar{n}_z/n_z v_{ion} + A}{1 + P} + k_\omega' + \Lambda_\omega \right\}, \quad (2)$$

$$I_{\omega p} = \frac{2\pi\hbar}{c^2} \omega^3 (\exp(\hbar\omega/T) - 1)^{-1},$$

where $I_{\omega p}$ is the spectral intensity of the equilibrium radiation; $k_{z\gamma}'$, k_ω' , and Λ_ω are the coefficients of photoabsorption of ions of charge z at the level γ , of the bremsstrahlung at

the frequency ω , and of the absorption in the lines;

$$R_{z\gamma} = \begin{cases} 0, & \hbar\omega < |E_\gamma| \\ v_w^{z+1}/v_r^{z+1}, & \hbar\omega \geq |E_\gamma| \end{cases}$$

E_γ is the energy of the level γ ,

$$A = \frac{n_z(v_r^z + v_w^z) - n_{z-1}v_{ion}^{z-1}}{n_z v_{ion}^z}.$$

Under the conditions considered, $A \approx 0$. In the derivation of (2) it was assumed that the electrons in the plasma have a Maxwellian distribution, the population of the discrete levels has a Boltzmann distribution, and the density of the ions is obtained from Eq. (1).

The quantities $R_{z\gamma}$ in (2) characterize the degree and character of the disequilibrium, and $\bar{n}_z/n_z v_{ion}^z$ characterizes the nonstationarity effects. By way of example we indicate the basic processes that determine the ionization states of a silicon ion in the corona at a temperature ~ 0.3 keV. The states of the K shell are determined by the competition between ionization by electron impact and by photorecombination, and the very same processes determine the state of the inner L -shell electrons, whereas for the outer L electrons the principal role is played by recombination in triple collisions. The deviation from equilibrium influences strongly the emission of hard photons with $\hbar\omega \gtrsim 2.5$ keV, inasmuch as $R_{z\gamma} \approx 250$ for the K shell.

Generation of "fast" electrons in the target corona leads to deviation of the x-ray spectrum from thermal at high photon energies. The fast-electron emission spectrum can be described under the following simple assumptions. The number of fast electrons in the target is given by

$$N_H \approx \alpha E_{abs} \tau / T_H, \quad \tau = m^2 v^3 / 2\pi e^4 n_i z_i (z_i + 5) \ln L,$$

where E_{abs} is the power of the absorbed laser radiation; α is the fraction of the absorbed laser energy that goes over into the fast-electron energy; τ is the characteristic slowing-down time of the fast electrons; m , e , and v are the mass, charge, and velocity of the electrons; $\ln L$ is the Coulomb logarithm; n_i and z_i are the density and the charge of the ions, and T_H is the fast-electron temperature in energy units. Since the fast electrons radiate from a corona region that is optically transparent to the hard photons, using the standard expression for the spectral emissivity connected with the bremsstrahlung mechanism¹⁰

$$I_\omega d\omega = \frac{32\pi}{3} \left(\frac{2\pi}{3T_H m} \right)^{1/2} \frac{z_i^2 e^6}{mc^3} n_i n_H e^{-\hbar\omega/T_H} d\omega.$$

We get for the time-integrated target spectral emission yield, determined by the fast electrons, the equation

$$E_\omega \left[\frac{J}{\text{keV}} \right] = 1.87 \cdot 10^{-5} \alpha E_{abs} \frac{z_i}{z_i + 5} \left(1 + 2.4 \frac{I_{z_i}}{T_H} \right) e^{-\hbar\omega/T_H}$$

(I_{z_i} is the ionization potential; T_H is in keV; E_{abs} is in J; the factor $2.4 I_{z_i}/T_H$ takes into account the contribution of the recombination radiation). The total yield of the target x-ray emission due to the fast electrons, $Q = \int E_\omega d\hbar\omega$, is proportional to the energy input αE_{abs} into the electron and to the electron temperature. It is necessary to choose $T_H \sim 10^{-5} (q\lambda^2)^{0.4}$ (Ref. 13), where q is the laser-radiation

TABLE I.

	E_{abs}, J	α	T_H, keV	Q_{exp}, J	Q_{calc}, J
"Kal'mar"	20	0.01	2.8	$7.5 \cdot 10^{-5}$	$2.2 \cdot 10^{-5}$
"Janus"	9	0.5	11.3	$6.2 \cdot 10^{-4}$	$3.7 \cdot 10^{-4}$
"Argus"	30	0.5	21.7	$3.9 \cdot 10^{-3}$	$1.4 \cdot 10^{-3}$

flux in W/cm^2 and λ is the wavelength in μm . The table lists the calculated and experimental values of Q for experiments performed in various regimes—the pusher shell regime ("Kal'mar") and the exploding shell regime ("Janus" and "Argus").¹⁴ In the exploding-shell regime the target x-ray yield due to the fast electrons is considerably higher than in experiments performed in the pusher shell regime (see the table).

The approach described above was used to develop a computer program for the calculation of the radiation from the target (code "RIM"), wherein the stationary radiation-transport equation is solved for specified space-time density and temperature profiles determined without allowance for the reaction of the radiation on the hydrodynamics in accord with the "Luch," "Rapid," and "ASAF" programs. This can be done, since the radiated energy is low. We have

$$\Omega \nabla I_{\omega} + \kappa'_{\omega} I_{\omega} = \epsilon_{\omega}, \quad (3)$$

where I_{ω} is the radiation intensity, κ'_{ω} is the absorption coefficient corrected for the stimulated emission,

$$\kappa'_{\omega} = \sum_{z, \tau} k_{z\tau} + k'_{\omega} + \Lambda_{\omega}.$$

The approximation using a stationary radiation field corresponding to the instantaneous distribution of the absorption and emission sources is valid, since the plasma velocity is much less than that of light.¹¹ Equation (3) was integrated over space by the method of characteristics. The "RIM" program makes it possible to determine by a single integration over space the spectrum of the radiation that emerges to the outside of the target

$$E(\omega) = \int_{S_{sur}} dS \int_{\Omega} I_{\omega} \Omega d\Omega;$$

the spatial distribution of the energy transferred from the radiation to the plasma in the transport process

$$Q(r) = \int d\omega \int \kappa'_{\omega} I_{\omega} \Omega d\Omega;$$

the angular distribution of the plasma intrinsic radiation, and the x-ray output from targets of various compositions and with different space-time distributions of the plasma parameters. The program incorporates blocks for the interpretation of the emitted radiation, which simulate the determination of the illumination of the target x-ray photograph on photographic film behind the aperture of the pinhole camera and the passage of the radiation through various filters.

§2. EXPERIMENTAL CONDITIONS AND X-RAY DIAGNOSTICS METHODS

The experiments were performed on the high-power nine-channel "Kal'mar" facility, a detailed description of

which is given in Ref. 15. The targets were spherical shells of Si_2O glass or polystyrene $(C_8H_8)_n$ filled with deuterium at pressure 10–30 atm. The target-preparation technology is described in Ref. 16.

The x-ray diagnostics methods used in these experiments can be divided into two groups: a) integral methods (without spatial resolution) and b) pinhole cameras that produce the image of the plasma with high ($\sim 10 \mu m$) spatial resolution.

Two integral methods were used: 1) reconstruction of the spectrum from the plots of the radiation absorption in the material; 2) reconstruction of the spectrum from photoelectron tracks in nuclear emulsion (this method is described in detail in Ref. 17).

In the first case, three types of detector were used: UV-VR photographic film, thermoluminescent detectors (TLD), and scintillators with photomultipliers.

A detector based on photographic film has important advantages: high sensitivity and possibility of performance of multichannel measurements, but its operating range is limited to the region $\hbar\omega \lesssim 10$ keV. In the $10 \lesssim \hbar\omega \lesssim 15$ keV range, the most suitable is a TLD: its sensitivity here is higher than that of a photographic film, and multichannel measurements are also technically easy to perform. The TLD calibration accuracy exceeds considerably the accuracy of the calibration of photographic film. This makes it possible, by comparing the readings of these detectors where their working ranges overlap, to increase the accuracy of the film detectors. Detectors based on scintillators with photomultipliers, while having a much higher sensitivity than the first two types, have a serious shortcoming, namely the technical difficulty of recording in a large number of channels. In our experiment these detectors were used therefore only to record the hard part of the spectrum ($\hbar\omega \gtrsim 15$ keV).

The use of all three types of detector thus enabled us to record signals in an intensity range of ~ 7 decades, corresponding to the use of filters from 400 μm of beryllium to 5 mm of aluminum, and making possible measurements in the spectral range from 2 to 25 keV.

The data on the absorption of the radiation by the filters were used to reconstruct the plasma x-ray spectrum by two independent methods. The first is described in detail in Ref. 18, where it is called the effective-energy method. The second method consists of solving the equation

$$M(x) = \int_{\lambda_1}^{\lambda_2} K(\lambda, x) s(\lambda) d\lambda. \quad (4)$$

Here $M(x)$ is the transmission coefficient of the investigated radiation as a function of the filter thickness x ; $K(\lambda, x)$ is the matrix of the attenuation coefficients of monochromatic radiation of wave length λ by detectors of thickness x ; λ_1 and λ_2 are the end points of the spectral band, and $s(\lambda)$ is the spectral density of the number of photons or of the radiation energy.

Equation (4) is a linear Fredholm integral equation of the first kind, and the problem of finding $s(\lambda)$ from the known $M(x)$ and $K(\lambda, x)$ belongs to the class of "incorrect" problems. In Ref. 19 is described a method, in the form of a

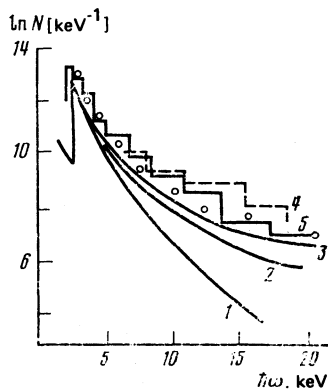


FIG. 2. Spectrum of continuous x radiation—number of photons of a given frequency, emitted by a target into 4π sr during the entire time of the pulse. 1—Results of calculation under the assumption that there are no fast electrons in the plasma ($T_H = 0$), 2 and 3—calculated spectra under the assumption that 1% of the absorbed energy was converted into fast-electron energy and that the electron temperatures are respectively $T_H = 2.5$ and $T_H = 3$ keV. Experimental data: spectrum reconstructed from photoelectron tracks in nuclear emulsion (4) or determined from absorption curves by the effective-energy method²¹ (5); points—values obtained by the method described in Ref. 19.

computer program, of solving problems of this type.

Figure 2 demonstrates the target x-ray spectrum obtained from theoretical calculations, reconstructed from photoelectron tracks in nuclear emulsion, and obtained by effective-energy method and by solving Eq. (4). It can be seen that all these curves are in good agreement.

The continuous x-ray spectrum was investigated with spatial resolution by using pinhole cameras that photographed the targets from different directions; the recording element was UF-VR x-ray photographic film. The substrate was a copper film $50 \mu\text{m}$ thick, opaque to radiation with photon energy $h\omega < 20$ keV. The minimum pinhole diameter was $\sim 7 \mu\text{m}$. The geometry of plasma photography in its own x rays was optimized (in aperture and resolution) by the method described in Ref. 15.

It must be noted that direct measurements of the energy of the target intrinsic radiation are difficult, since this radiation is considerably weaker than the scattered laser radiation. The total radiation energy can be approximately estimated from the readings of an uncovered TLD; it follows from these readings that this energy does not exceed 0.2 J ($\sim 1\%$ of the absorbed energy).

§3. DISCUSSION OF EXPERIMENTAL RESULTS. COMPARISON WITH THEORY AND WITH CALCULATIONS

In the analyzed experiments the shell targets, glass or polystyrene, of radius $R_0 \approx 70\text{--}100 \mu\text{m}$ and wall thickness $\Delta R_0 \approx 2\text{--}7 \mu\text{m}$, were filled with deuterium and irradiated from all sides by a flux $q \sim 10^{14}$ W/cm² from a neodymium laser at an energy 100–200 J and pulse duration (at the base) $\tau_{\text{pul}} \approx 1\text{--}2.5$ nsec. The energy absorbed in the target was 20–40 J.²⁰ The x-ray diagnostics methods used in the “Kalmar” facility²¹ were designed for the frequency range of intrinsic radiation higher than 2 keV.^{6,21} In this frequency interval the investigated targets produced no radiation due to bound-bound transitions, i.e., there was only a continuous spectrum.

We present below the results of calculation of the radiation field of a glass shell target with parameters $R_0 = 70 \mu\text{m}$, $\Delta R_0 = 2 \mu\text{m}$, $m_{D_2} = 6.32 \times 10^{-9}$ g, $E_{\text{abs}} = 20$ J, and $\tau_{\text{pul}} = 2.5$ nsec. We obtained a space-time picture of the ionization, time-integrated spectra of the x rays, and pinhole-camera picture of the target. In the course of contraction, regions of rarefied hot corona, of a cold compressed shell, and of a hot dense core are produced in the target. Contributing to the integral plasma luminosity are the corona zone near the critical surface and the target central region heated and compressed as a result of spherical cumulation. The maximum of the corona emission is shifted away from the critical surface towards the center of the targets where the densities are higher. The glow time of this region is comparable with the duration of the laser pulse, and the evolution in space is similar to the displacements of the critical surface. The emission in the corona is directly dependent on the absorbed laser energy—the larger the latter, the higher the corona temperature and the larger its emissivity. The emission time of the central region is of the order of the time of confinement of the gas in the compressed state and amounts to $\sim 10^{-10}\text{--}10^{-15}$ sec. The main contribution is made by the radiation of the heated shell layers adjacent to the gas. Figure 2 shows the spectrum of the radiation from the target. It should be noted that if no account is taken of the disequilibrium effect, the curve calculated for $h\omega > 2.5$ keV would lie higher by two orders of magnitude. The total intrinsic radiation energy for the target considered is $\sim 4\%$ of the absorbed energy, a value that does not contradict the experimental data. At energies $h\omega \geq 8$ keV the decisive role is played by the radiation due to the fast electrons produced in the critical-density region with $T_H \approx 3$ keV. Agreement between the experimental and calculated spectra is reached when the total energy of the fast electrons is 1% of the absorbed, in accord with the resonant-absorption contribution determined with the “Rapid” program.⁹

The radiation generated in the corona region goes both to the outside and to the interior of the target, heating the outer region of the compressed but relatively cold shell. For the target with the parameters cited above, ~ 0.1 J of the

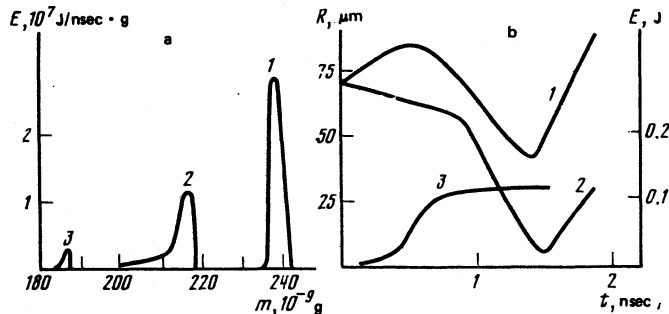


FIG. 3. a) Contribution of intrinsic radiation energy of the corona into the shell target at various instants of time. Curve 1 corresponds to 0.506 nsec, 2—0.775 nsec, 3—1.377 nsec (the instant of collapse of the shell). Initial shell mass 2.70×10^{-9} g. b) R - t diagram of motion of critical surface (1) and boundaries of deuterium core (2), 3—time dependence of energy of intrinsic corona radiation absorbed by the shell.

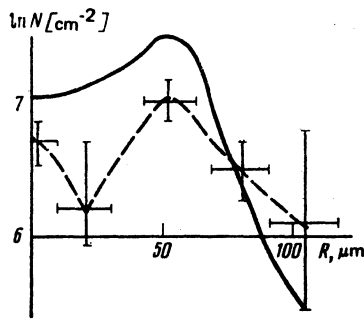


FIG. 4. Spatial distribution of illumination on a photographic plate behind the aperture of a pinhole camera (diameter $15 \mu\text{m}$), produced by the intrinsic radiation of the target plasma. Dashed line—experimental curve, solid—calculation result.

intrinsic radiation ($\sim 0.5\% E_{\text{abs}}$) is absorbed by the instant of maximum shell compression (Fig. 3).

Figure 3a shows the time evolution of the shell heating by this radiation. At each instant of time not more than 4%

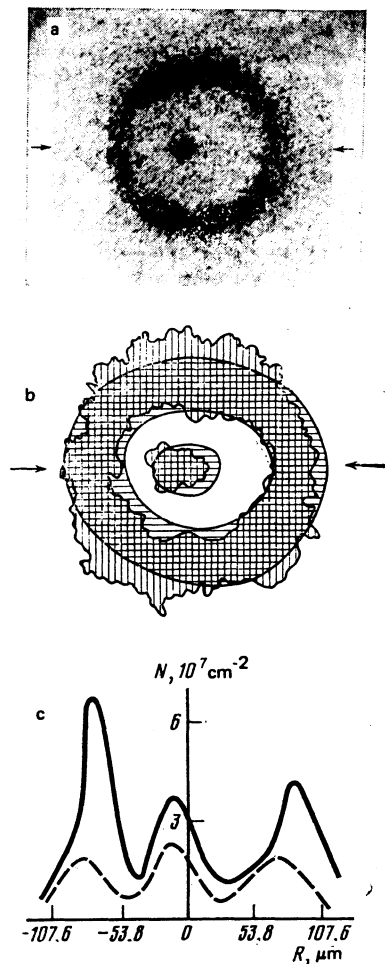


FIG. 5. X-ray pinhole photograph (a) and density pattern of its diametrical cross section (c). Dashed line—experiment, solid—calculation. In Fig. b, the calculated regions of the emission of the core and of the target corona (horizontal hatches) are superimposed on the target emission regions obtained as a result of the reduction of the pinhole photography (vertical hatches).

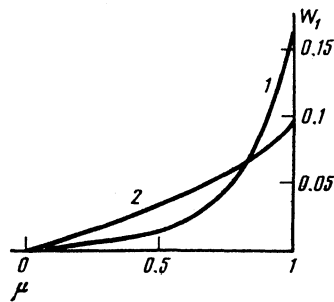


FIG. 6. Dependence of the power absorbed in one solid angle on $\mu = \cos \theta$, where θ is the angle reckoned from the optical axis from the beam. Curve 1—without allowance, 2—with allowance for refraction. This distribution is produced by a single laser beam. The incident laser beam had a Gaussian intensity distribution over the beam radius. The characteristic beam radius on the target was equal to the initial target radius.

of the shell mass is heated. This leads to a larger evaporation of the shell and to a negligible increase of the corona mass. This heating does not influence the compression.

As indicated in §2, to determine the volume compression of the deuterium we registered in the experiments the continuous plasma x rays with pinhole cameras. Figure 4 shows the experimental and calculated time-integrated spatial distribution of the illumination produced on photographic film behind the pinhole by the intrinsic radiation of the plasma target (with photon energy $\hbar\omega \gtrsim 2.5 \text{ keV}$). The calculation accounts well for the locations of the regions of the illumination from the corona and from the center.

Pinhole photography of the plasma in its own x rays gives a clear idea of the compression symmetry. Figure 5a shows a photograph of the plasma with a pinhole camera at a spatial resolution $10 \mu\text{m}$ ($\hbar\omega \sim 2 \text{ keV}$) for a polystyrene shell of diameter $2R_0 = 179 \mu\text{m}$ and wall thickness $6.9 \mu\text{m}$, $E_{\text{abs}} = 17 \text{ J}$, $\tau_{\text{pul}} = 2.5 \text{ nsec}$. Besides the outer quite symmetrical glowing region of the corona one can see the central region, which is strongly shifted relative to the geometric center of the corona emission—a glowing polystyrene layer adjacent to the compressed gas.

Since the target was not symmetrically irradiated in this experiment, the self-consistent calculation of the energy release and of the hydrodynamics of target-plasma compression is essentially a three-dimensional problem. The target-illumination symmetry was determined in this experiment with the "Rapid" program with allowance for the real irradiation geometry and for the irradiation energy in each of the nine beams.⁹ Figure 6 shows the distribution of the absorbed power when a spherical target is illuminated by a single beam, without and with allowance for refraction. The symmetrizing influence of the refraction can be seen. Similar results were obtained also when the target was illuminated by all nine beams. The distribution of the laser radiation luminosity on the target surface has no axial symmetry, but a three dimensional calculation is at present impossible. This experiment was therefore numerically simulated using a two-dimensional axisymmetric calculation in accord with the "ASAF" program, wherein the spherically symmetrical target was illuminated by an inhomogeneous flux averaged

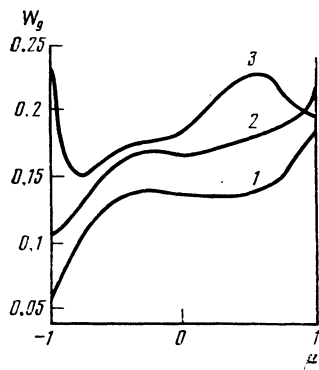


FIG. 7. Angular distribution of power absorbed per unit solid angle at various instants of time following irradiation of the target by nine beams. Curve 2 corresponds to $t = 0.498$ nsec, 2—0.806 nsec, 3—2 nsec.

over the angle φ and distributed over the azimuthal angle θ in accord with Fig. 7.

Figure 8 shows the results of the two dimensional calculation at one of the instants of time; on the left is shown, to a larger scale, the contracting central part of the target. Owing to the strong asymmetry of the incident flux—the laser-radiation flux on the lower hemisphere exceeds the one on the upper by 30%—the glowing core is shifted away from the geometric center of the target. The luminous target regions shown in Fig. 5b were obtained by reducing an experimental pinhole photograph (Fig. 5a), and superimposed on them are time-integrated calculated luminous regions of the core and of the corona of the target. In the lower part (Fig. 5c) are shown plots of the calculated and experimental luminosity of the pinhole photographs in the cross section marked by the arrows. Even though the three-dimensional picture of the heating and compression was simulated with a two-dimensional calculation, the locations of the luminous regions of the central part and of the corona, obtained by this method, agree with the experimental data.

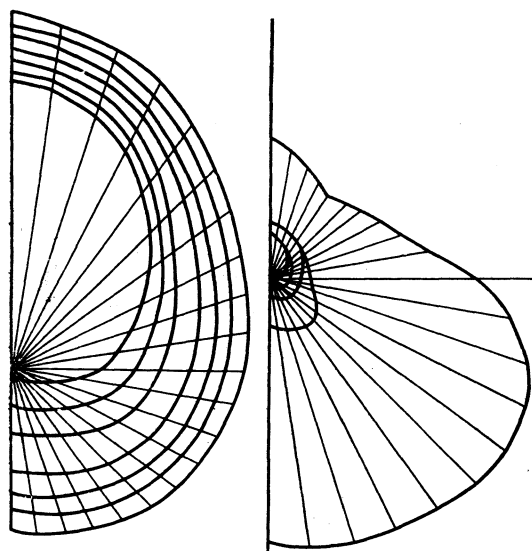


FIG. 8. Deformation of spherically symmetric gasdynamic cells in the course of compression by an asymmetric laser flux. The figure shows the instant of maximum compression.

What is noteworthy is the high symmetry of the compression at a strong asymmetry of the irradiation at moderate fluxes ($\sim 10^{14}$ W/cm²), although the loss of density of the compressed target core is approximately 40% compared with the spherically symmetrical case. This is due, first, to the dynamic mismatch of the compression with time, since different parts of the compressing cold shell do not reach the smallest values of their radii simultaneously. A second factor that decreases the compression is the large entropy introduced into the gas by the shock wave in the case of asymmetric compression, compared with symmetric, and this in turn hinders the compression. Nevertheless, even in the presence of these unfavorable factors the degree of compression remains high and reaches ~ 1000 in this case.

CONCLUSION

Our analysis of the x radiation supplements the picture presented in Refs. 1 and 5, of the heating and compression of shell targets irradiated by a nanosecond laser pulse in experiments on the "Kal'mar" facility at moderate irradiances, $\sim 10^{14}$ W/cm². At a laser energy ~ 100 J, in shells 100–200 μ m in diameter, not more than 5% of the absorbed laser energy in the case of glass shells, and a fraction of one percent in the case of organic-material shells, goes over into x rays in the course of heating, compression, and expansion. Under the conditions of these experiments, the intrinsic radiation does not affect the compression. The ionization in the corona is a nonequilibrium and nonstationary process. The spectrum of the emitted radiation is strongly influenced by the disequilibrium of the ionization and by the presence of fast electrons in the target corona. Two-dimensional simulation of experiments with substantial irradiation inhomogeneity makes it possible to obtain pinhole photographs that agree with the experimental ones, i.e., a two-dimensional calculation accounts correctly for real heating and compression of laser targets.

Thus, the results reported in the present article confirm the conclusion drawn in Refs. 1 and 5 that it is possible to describe the "Kal'mar" experiments within the framework of a hydrodynamic model with classical transport processes. The data presented on the spectrum and amount of the x radiation following irradiation of glass targets of ~ 100 μ m diameter by laser radiation flux $\sim 10^{14}$ W/cm² (average quantum energy ~ 0.5 to 1 keV) can be useful in the assessment of the possibility of using a laser plasma as a source of x rays for lithography purposes.²² It must be noted that with increasing ion charge the x-ray yield from the plasma decreases. The "RIM" program makes it possible to determine the parameters of this radiation for arbitrary experimental conditions.

¹Yu. V. Afanas'ev, N. G. Basov, B. L. Vasin, *et al.*, *Zh. Eksp. Teor. Fiz.* 77, 2539 (1979) [*Sov. Phys. JETP* 50, 1229 (1979)].

²N. G. Basov, A. A. Kologrivov, O. N. Krokhin, *et al.*, *Pis'ma Zh. Eksp. Teor. Fiz.* 23, 474 (1976) [*JETP Lett.* 23, 428 (1976)].

³Yu. V. Afansiev, N. G. Basov, P. P. Volosevich, *et al.*, *Plasma Physics and Controlled Nuclear Fusion Research*, IAEA, Vienna, 1975, Vol. 2, p. 559.

⁴N. G. Basov, O. N. Krokhin, G. V. Sklizkov, *et al.*, *Zh. Eksp. Teor. Fiz.* 62, 203 (1972) [*Sov. Phys. JETP* 35, 109 (1972)]. N. G. Basov, Yu. A.

- Zakharenkov, N. N. Zorev, *et al.*, Zh. Eksp. Teor. Fiz. 71, 1788 (1976) [Sov. Phys. JETP 44, 938 (1976)].
- ⁵N. G. Basov, P. P. Volosevich, E. G. Gamaliĭ, *et al.*, Zh. Eksp. Teor. Fiz. 78, 420 (1980) [Sov. Phys. JETP 51, 212 (1980)].
- ⁶Yu. V. Afanasiev, N. G. Basov, N. N. Demchenko, *et al.*, Laser Interaction and Related Plasma Phenomena, Vol. 5, (H.J. Schwarz, H. Hora, M. Lubin, and B. Yaakoby, eds.), Plenum, 1981, p. 517.
- ⁷Yu. V. Afanas'ev, G. A. Vergunova, P. P. Volosevich, *et al.* Trudy FIAN 134, 103 (1982).
- ⁸P. P. Volosevich, L. M. Degtyarev, E. I. Levanov, *et al.* Fiz. plazmy 2, 883 (1976) [Sov. J. Plasma Phys. 2, 491 (1976)].
- ⁹Yu. V. Afanas'ev, E. G. Gamaliĭ, N. N. Demchenko, *et al.* Zh. Eksp. Teor. Fiz. 79, 837 (1980) [Sov. Phys. JETP 52, 425(1980)].
- ¹⁰Yu. V. Afanas'ev, P. P. Volosevich, E. G. Gamaliĭ, *et al.*, Pis'ma Zh. Eksp. Teor. Fiz. 23, 470 (1976) [JETP Lett. 23, 425 (1976)].
- ¹¹Ya. B. Zel'dovich and Yu. P. Raizer, Physics of Shock Waves and High Temperature Hydrodynamic Phenomena, Academic, 1966, Chaps. 2 and 6.
- ¹²L. A. Vainshteĭn, I. I. Sobel'man, and E. A. Yukov, Vozbuzhdenie atomov i ushirenie spektral'nykh liniĭ (Excitation of Atoms and Broadening of Spectral Lines), Nauka, 1979, Chap. 1.
- ¹³Laser Programme Annual Report, LLL, 1979.
- ¹⁴Laser Programme Annual Report, LLL, 1976.
- ¹⁵B. L. Vasin, A. A. Erokhin, N. N. Zorev, *et al.*, Trudy FIAN 133, 51 (1983).
- ¹⁶A. I. Isakov, Yu. A. Merkul'ev, and A. I. Nikitenko, Trudy FIAN 127, 62 (1980).
- ¹⁷V. V. Kushin, V. K. Lyapidevskii, Yu. A. Mikhailov, *et al.*, FIAN Preprint No. 72, 1979.
- ¹⁸S. A. Zverev, G. V. Kon'kova, V. K. Lyapidevskii, *et al.* in: Meditsinskaya radiatsionnaya tekhnika (Medical Radiation Techniques), Moskovskaya pravda, 1978, p. 26.
- ¹⁹A. A. Kologrivov, G. V. Sklizkov, and A. S. Shikanov, FIAN Preprint No. 142, M., 1981.
- ²⁰N. G. Basov, A. A. Erokhin, Yu. A. Zakharenkov, *et al.*, Pis'ma Zh. Eksp. Teor. Fiz. 26, 581 (1977) [JETP Lett. 26, 433 (1977)].
- ²¹A. A. Erokhin, S. A. Zverev, A. A. Kologrivov, *et al.*, Kratk. Soobshch. Fiz. No. 9, 27 (1979).
- ²²G. Dahlbacka, S. M. Matthews, R. Strigield, *et al.*, in: Low Energy X-ray Diagnostics (D. T. Attwood and B. L. Henke, eds.), AIP Conf. Proc. No. 75, p. 22 (1981).

Translated by J. G. Adashko